EMBRY-RIDDLE
Aeronautical University
SCHOLARLY COMMONS

Aerospace Engineering - Daytona Beach | College of Engineering

3-2009

Molecular Dynamics Study of Crystal Plasticity during Nanoindentation in Ni Nanowires

V. Dupont
Embry Riddle Aeronautical University, dupontv@erau.edu

F. Sansoz
The University of Vermont

Follow this and additional works at: https://commons.erau.edu/db-aerospace-engineering

 Part of the Aerospace Engineering Commons

Scholarly Commons Citation

Dupont, V., & Sansoz, F. (2009). Molecular Dynamics Study of Crystal Plasticity during Nanoindentation in Ni Nanowires. *Journal of Materials Research, 24*(3). Retrieved from https://commons.erau.edu/db-aerospace-engineering/3

This Article is brought to you for free and open access by the College of Engineering at Scholarly Commons. It has been accepted for inclusion in Aerospace Engineering - Daytona Beach by an authorized administrator of Scholarly Commons. For more information, please contact commons@erau.edu.

Molecular dynamics study of crystal plasticity during nanoindentation in Ni nanowires

V. Dupont and F. Sansoz[a)]
School of Engineering, The University of Vermont, Burlington, Vermont 05405

(Received 31 July 2008; accepted 28 October 2008)

Molecular dynamics simulations were performed to gain fundamental insight into crystal plasticity, and its size effects in nanowires deformed by spherical indentation. This work focused on <111>-oriented single-crystal, defect-free Ni nanowires of cylindrical shape with diameters of 12 and 30 nm. The indentation of thin films was also comparatively studied to characterize the influence of free surfaces in the emission and absorption of lattice dislocations in single-crystal Ni. All of the simulations were conducted at 300 K by using a virtual spherical indenter of 18 nm in diameter with a displacement rate of 1 $m \cdot s^{-1}$. No significant effect of sample size was observed on the elastic response and mean contact pressure at yield point in both thin films and nanowires. In the plastic regime, a constant hardness of 21 GPa was found in thin films for penetration depths larger than 0.8 nm, irrespective of variations in film thickness. The major finding of this work is that the hardness of the nanowires decreases as the sample diameter decreases, causing important softening effects in the smaller nanowire during indentation. The interactions of prismatic loops and dislocations, which are emitted beneath the contact tip, with free boundaries are shown to be the main factor for the size dependence of hardness in single-crystal Ni nanowires during indentation.

I. INTRODUCTION

Quasi-one-dimensional metal nanowires[1] are the building blocks for nanoscale research in a vast variety of disciplines that range from biology to electromechanics and photonics.[2–5] These nanomaterials have recently stimulated the interest of the mechanics community, because most experimental evidence shows a strong influence of the sample dimension on the mechanical properties of metals at nanometer scale.[6–11] Whereas the strength and ductility of metals in macroscopic samples are predominantly determined by the relevant microstructure length scale (e.g., grain size), which is often small relative to the sample size, a distinctive behavior of crystal plasticity emerges in metal nanostructures, where the material strength significantly increases as the deformation length scale (diameter or volume) decreases. A microplasticity mechanism has been proposed to account for the size scale dependence of small metallic samples based on dislocation starvation, in which the density of mobile dislocations created from pre-existing dislocation sources is counter-balanced by the density of dislocations escaping the crystal at free surfaces.[7,10,12] The in situ TEM compression experiments of Shan et al.[13] have recently confirmed this mode of deformation in Ni nanopillars as small as 150 nm in diameter. Nevertheless, it remains crucial to characterize the influence of sample size on dislocation activity at even smaller length scale (<100 nm) to achieve meaningful results on the crystal plasticity of metal nanowires.

Nanoindentation technique via pillar compression method[6,7,9–11,13] has enabled rapid progress in the experimental investigation of nanomechanical properties and their size dependence in metals at the micron and submicron scales. However, the nanopillar compression method has never been applied to samples less than 100 nm in diameter due to complications in preparation and mechanical testing at such a small scale. By contrast, the use of nanoindentation tips to probe the radial elastic modulus and hardness of sub-100 nm nanowires has been found successful in the past.[14–22] Whereas a fundamental understanding of dislocation activity during metal nanopillar compression has already been supplemented by atomistic simulations,[23–27] the atomic mechanisms of plasticity and related size effects for metal nanowires deformed by nanoindentation remain elusive.

The aim of this work is to elucidate the processes of plastic deformation in metal nanowires subjected to nanoindentations by atomistic simulation. To this end, large-scale molecular dynamics simulations are performed to provide atomistic insight into the size dependence of mechanical properties in [111]-oriented single-crystal, defect-free Ni nanowires deformed by

[a)]Address all correspondence to this author.
e-mail: frederic.sansoz@uvm.edu
DOI: 10.1557/JMR.2009.0103

 © 2009 Materials Research Society

spherical indentation. The significance of dislocation activity in the absence of free-surface boundaries is also addressed by using nanoindentation simulations on single-crystal Ni thin films. A comparative study of the effects of sample size and free surfaces between thin film and nanowires is presented. The atomic mechanisms of plastic deformation related to the emission of lattice dislocations and their absorption by free surfaces during indentation are also analyzed.

II. SIMULATION METHODS

Parallel molecular dynamics simulations were performed to study the nanoindentation of single-crystal Ni thin films and nanowires deformed by a frictionless, spherical tip of 18 nm in diameter (Fig. 1). Simulations were conducted on [111]-oriented single-crystal Ni nanowires with a cylindrical shape. The nanowires were 40 nm in length, and either 30 or 12 nm in diameter as illustrated in Figs. 1(b) and 1(d), respectively. Periodic boundaries were only applied along the wire axis. To simulate thin films, the whole simulation box (40 × 40 nm) was filled with atoms and periodic boundary conditions were applied to the directions parallel to the film surface [Fig. 1(a)]. Two films of 30 and 12 nm in thickness as shown in Figs. 1(a) and 1(c), respectively, were investigated. We have also verified that the boundary conditions of our thin-film models did not influence the results by simulating the nanoindentation of a larger model of thickness 12 nm and size 60 × 60 nm (data not shown). For

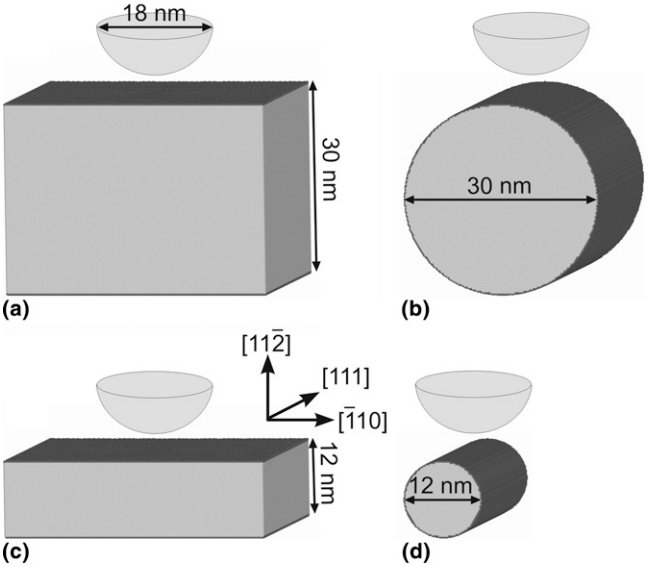

FIG. 1. Atomistic models of spherical indentation for thin films and nanowires. The diameter of the virtual indenter is 18 nm. (a) 30-nm-thick film. (b) 30-nm-diameter nanowire. (c) 12-nm-thick film. (d) 12-nm-diameter nanowire. The crystallographic orientation of the films and nanowires is as indicated. Free surfaces appear in dark-gray, whereas atoms in FCC lattice are colored in light-gray.

both thin-film and nanowire models, the indentation was performed along the [11$\bar{2}$] crystallographic direction of the sample, and the bottom two atomic layers were fixed along the direction of indentation. In addition, the bottom two atomic layers in the nanowires were constrained along the [$\bar{1}$10] direction, normal to the direction of indentation, to prevent the wire from rolling during the deformation. The total number of atoms ranged from 400,000 (12-nm-diameter nanowire) to 4.4 million (30-nm-thick film). The embedded-atom method (EAM) interatomic potential for Ni from Mishin et al.[28] was used. This potential has been fitted on ab initio calculations and experimental values, which improves the prediction of surface energies and stacking fault energies for Ni. The simulations were performed at 300 K by using a NVT integration scheme with a time step of 5 fs. Similar to past atomistic studies,[29,30] the virtual indenter was modeled by a spherical, repulsive force of magnitude

$$F(r) = -k(r - R)^2 \quad , \tag{1}$$

where r is the distance from an atom to the center of the indenter, R is the radius of the indenter, and k is a force constant (= 10 N/m^2). A gap of 0.2 nm was initially imposed between the sample surface and the indenter. The indenter was displaced at a rate of 1 m/s. Despite being unrealistically high, such a velocity used in our simulations is relatively small in comparison with the range of strain rates achievable by current molecular dynamics simulations.[29,30] The final depth of indentation into the samples was 1.8 nm (400,000 steps). The atomic positions were recorded at 50 ps intervals (10,000 steps). The local lattice structure was determined from the formulation given by Ackland and Jones.[31] In this paper, atoms in dark-gray color represent surface and noncoordinated atoms, whereas atoms in HCP configuration (stacking faults) appear in light-gray color. For most figures, in the following, atoms in FCC configuration have been omitted for clarity.

The contact zone was defined by the atoms positioned within the boundary of the indenter (i.e., $r < R$). As such, the mean contact pressure p_m was calculated as

$$p_m = \frac{P}{A} \quad , \tag{2}$$

where P is the total load applied by the indenter to the contacted atoms, and A is the projected contact area, which was directly observed in the samples. In our atomistic simulations, it was found that the shape of the contact area was irregular, due to the discrete number of atoms; but for simplicity, the contact area was approximated by an elliptical shape following the model proposed by Feng et al.[18] for the nanoindentation of nanowires. The Young's modulus E was determined from each simulation by using the Hertz theory for

elastic circular contacts. According to this theory, the contact load P is related to the penetration depth δ by[32]:

$$P = \frac{4}{3}\sqrt{RE^*}\delta^{\frac{3}{2}} \quad , \tag{3}$$

where

$$\frac{1}{R} = \frac{1}{R_i} + \frac{1}{R_f} \quad , \tag{4}$$

with R_i and R_f, the tip radius and wire radius, respectively ($R_f = \infty$ for thin film), and

$$E^* = \frac{E}{1 - \nu^2} \quad , \tag{5}$$

with ν the Poisson's ratio, taken equal to 0.312 for Ni.[33] Each simulated force-displacement curve was fitted from the origin to the yield point by the following equation:

$$P = C\delta^{\frac{3}{2}} \quad , \tag{6}$$

from which E can be obtained such as

$$E = \frac{3(1 - \nu^2)}{4\sqrt{R}}C \quad . \tag{7}$$

The yield point was defined by the emission of the first dislocation after the elastic regime. For that purpose, further snapshots near the yield point were recorded at 0.5 ps intervals to capture this event. The mechanisms of dislocation nucleation under the indenter were also analyzed using the calculations of the local von Mises strain between two atomic configurations in the atomistic configuration viewer AtomEye.[34]

III. RESULTS

A. Elastic behavior and limit of elasticity

The force-displacement nanoindentation curves related to the atomistic models investigated are shown in Fig. 2. The evolution of these curves in the elastic regime is found to follow a Hertzian behavior in both thin films and nanowires. For example, Fig. 2 shows an excellent fitting between Hertzian theory, as given by Eq. (6), and atomistic results for a 30-nm-thick film, up to the yield point. The Young's moduli E determined by fitting Eq. (6) to the atomistic results are provided in Table I. This table shows, in both thin films and nanowires, that the E value decreases by approximately 3.7% as the sample size decreases from 30 to 12 nm. Similarly, the E value decreases by 2.4% with the introduction of free surfaces, from films to nanowires. The mean value of Young's modulus is found equal to 291 ± 7.5 GPa. The latter shows that the variations in Young's modulus are relatively small, which is consistent with the results of Liang et al.[35] for the Young's modulus of [111] nanowires. The mean E value is also found to be larger than that for bulk Ni in the [112] direction calculated from the stiffness matrix associated with the potential (232 GPa).[28] This confirms the results of Cuenot et al.,[36] who found that the value of the Young's modulus for different metallic nanowires was larger than bulk values for diameters less than 100 nm.

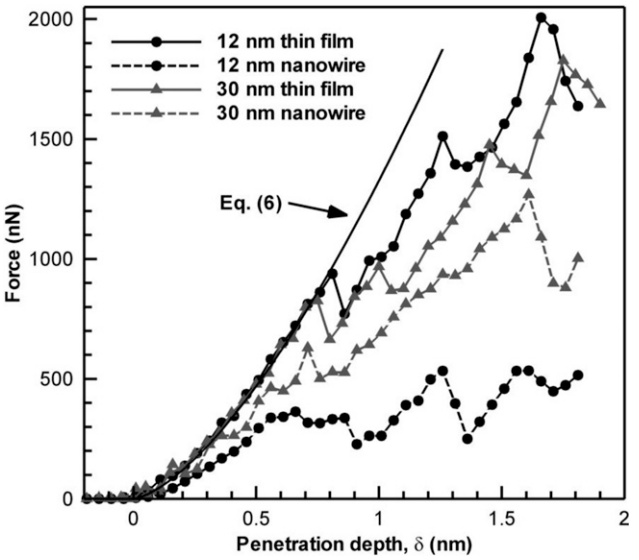

FIG. 2. Simulated force-displacement nanoindentation curves for Ni thin films and nanowires indented by a spherical tip. Equation (6) fitted to the 30-nm-thick film model is also represented.

TABLE I. Young's modulus and mechanical characteristics at yield point in Ni thin films and nanowires from molecular dynamics simulations of spherical indentation.

			Mechanical characteristics at yield point	
Sample	Thickness/ diameter (nm)	E (GPa)	Contact force (nN)	Mean contact pressure, p_m (GPa)
Film	30	300	824.5	29.6
	12	289	938.7	29.3
Nanowire	30	293	629.1	32.7
	12	282	338.2	31.0

Furthermore, Table I reveals that the contact force at yield point is less significant in nanowires than in thin films. This result may be attributed to the fact that the slope of the force-displacement curves in the elastic range and the depth of indentation at yield point are smaller for nanowires, as shown in Fig. 2. However, the change in mean contact pressure p_m determined at the limit of elasticity is negligible between nanowires and thin films. The mean contact pressures obtained in our models (30.6 ± 1.5 GPa) are found to be consistent with the atomistic results of Nair et al.,[37] who predicted that the contact pressure necessary to emit the first

dislocation during spherical indentation of [111]-oriented Ni films with thickness varying from 4 to 12.8 nm is approximately 28 GPa.

B. Plastic behavior in thin films

The evolution of mean contact pressure as a function of penetration depth in films of different thicknesses is represented in Fig. 3(a). This figure shows that the plastic flow in thin films after yielding presents a serrated behavior, characterized by a series of drops in contact pressure. However, it is also shown in Fig. 3(a) that the evolution of the contact pressure for both films tends to a constant hardness H, which is found to be on the order of 21 GPa, after a penetration depth of 0.8 nm. This result therefore demonstrates that the film thickness does not significantly influence the hardness of the films investigated.

Furthermore, the atomic-level analysis of deformation mechanisms in thin films is presented in Fig. 4. Figures 4(a) and 4(c) show that the onset of plasticity is related to the emission of several half-dislocation loops in the {111}<110> slip system under the indenter. These two figures also point out to the conclusion that the deformation mechanism at the onset of plasticity is almost identical, regardless of the film thickness.

For larger plastic deformation, several dislocations detach themselves from the contact interface to create four-sided prismatic loops.[38] Such prismatic loops are then found to propagate through the thickness of the films. At the final stage of indentation in the 12-nm-thick film [Fig. 4(b)], it can be noticed that one prismatic loop and several {111} dislocation loops emitted from the contact zone are blocked by the lower boundary of the film, which is fixed. The formation and pile-up of several prismatic loops is more evident in the 30-nm film than the 12-nm film in the lower part of the model [Fig. 4(d)].

C. Plastic behavior in nanowires

Similar to the thin film models, it is shown in Fig. 3(b) that several drops in mean contact pressure occur after yielding in Ni nanowires during the indentation.

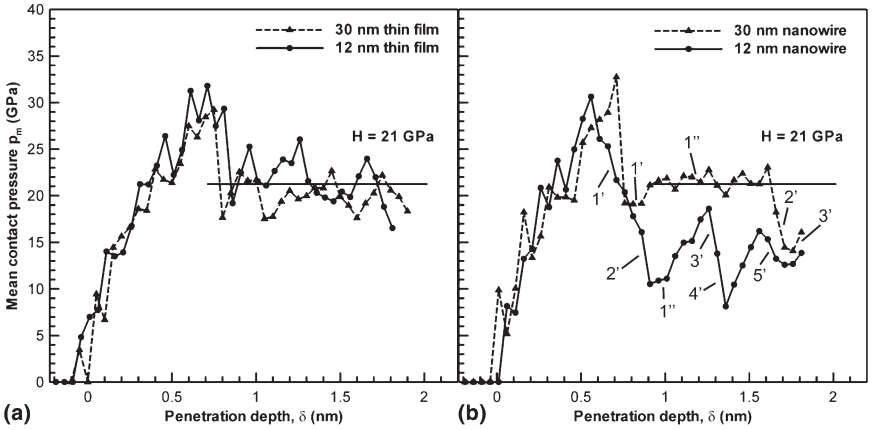

FIG. 3. Evolution of the mean contact pressure as a function of penetration depth in (a) thin films and (b) nanowires. The numbers (1-5) indicate the events of dislocation absorption by free surfaces in the nanowires. The prime and double prime symbols are used to designate slip on different slip systems.

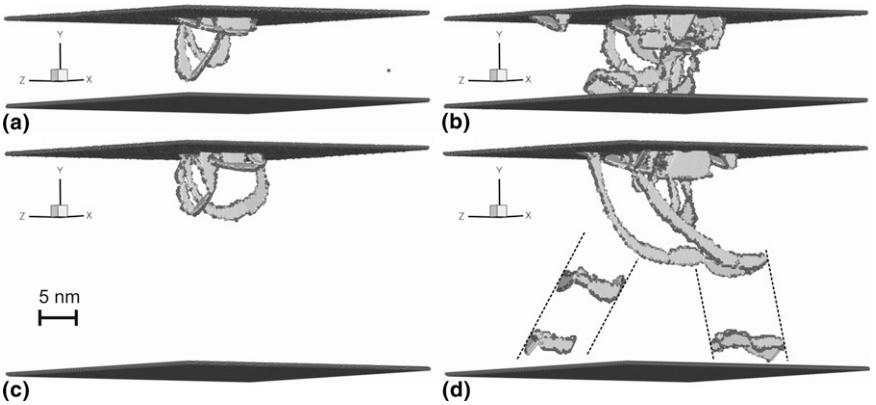

FIG. 4. Atomic-level representation of plastic deformation in Ni thin films during spherical indentation. (a) 12-nm-thick film at yield point. (b) 12-nm-thick film at maximum indentation depth. (c) 30-nm-thick film at yield point. (d) 30-nm-thick film at maximum indentation depth. Dashed lines represent the trajectory of prismatic dislocation loops. X = [111]; Y = $[11\bar{2}]$; Z = $[\bar{1}10]$.

However, this serration effect appears to be more pronounced in the 12-nm nanowire than the 30-nm nanowire. Furthermore, we observe that the hardness of the 30-nm nanowire, as obtained after a penetration depth of 0.8 nm, is almost identical to the hardness of thin films (i.e., H = 21 GPa). In contrast, the 12-nm nanowire promotes smaller contact pressures than the 30-nm nanowire at a large depth of indentation. This observation therefore suggests that sample-size effects exist in the hardness of [111]-oriented single-crystal Ni nanowires, as opposed to the behavior observed in thin films. The size effect encountered on nanowires in the present study is characterized by a decrease of hardness, or softening effect, as the wire diameter decreases.

We observe that the major drops in contact pressure for nanowires can be correlated to the absorption of gliding dislocations by free boundaries, rather than by the nucleation of new dislocations. In particular, for the 12-nm-diameter nanowire, three significant drops can be noticed on the contact pressure-displacement curve in Fig. 3(b). The number of dislocations absorbed by the free surface is also shown in this figure, where the prime and double prime symbols are used to designate slip on different slip systems on either sides of the tip. During the first drop in the curve, several half-dislocation loops, similar to the loop shown in Figs. 5(a) and 5(b), are emitted on the $(\bar{1}11)[110]$ slip system. Two of those dislocations have been absorbed by the free surface during this event ($1'$ and $2'$). The other two drops correspond to further absorption of half loops by the free surface on the same slip system than above ($3'$-$4'$ and $5'$); see also Figs. 5(c) and 5(d).

However, it is important to note that the drops on the contact pressure-displacement curve are less significant during the absorption of the first dislocation, as opposed to other dislocations gliding on the same slip system. For example, in the 30-nm nanowire, three four-sided prismatic loops are absorbed by the free boundary, but only the effect of the last absorption event ($2'$) is visible on the curve in Fig. 3(b) ($1.6\ \text{nm} < \delta < 1.7\ \text{nm}$). This effect may be attributed to the fact that only the first ($1'$) and third ($2'$) prismatic loops in this simulation emanate from the same slip system, and have been absorbed at the same location on the surface (on the left side of the indenter), as highlighted in dashed line in Figs. 6(c) and 6(d).

There is also clear evidence from Fig. 5(c) that a larger number of steps have been formed on the surface of the 12-nm-diameter nanowire compared with the 30-nm-diameter nanowire shown in Fig. 6(c). This observation suggests that the process of dislocation absorption by the free surface is different between the two nanowires. To corroborate this hypothesis, we summarize in Table II the net number of dislocations nucleated under the tip and subsequently absorbed by the free surface, by differentiating both half-dislocation loops and four-sided prismatic loops. First, this table confirms that a similar number of dislocations are nucleated in both nanowires (10 and 11), which is consistent with the conclusion that the nucleation process does not change with the sample size. Furthermore, the table shows that the 12-nm nanowire only

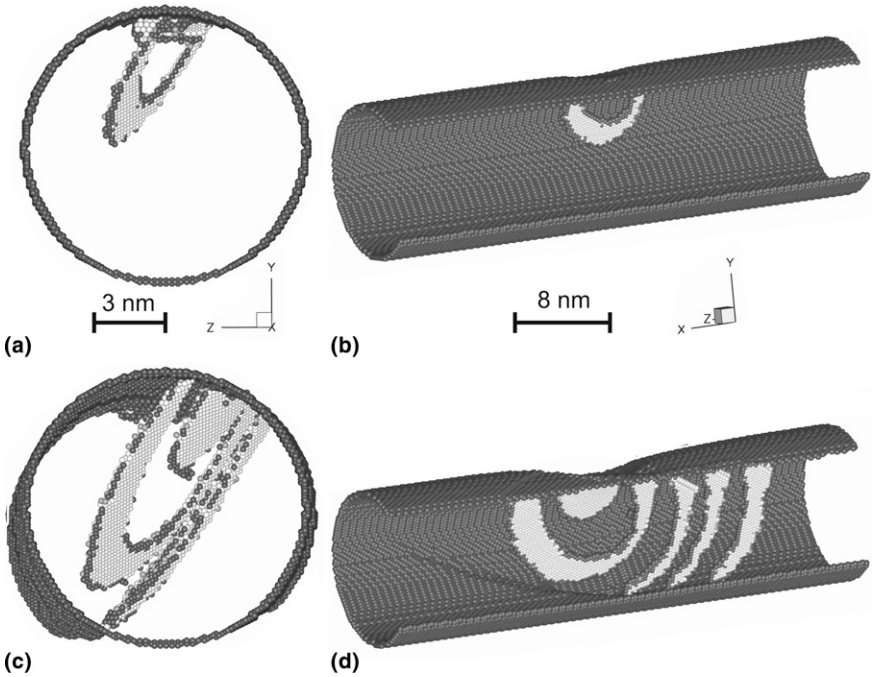

FIG. 5. Atomic-level representation of plastic deformation in a 12-nm-diameter Ni nanowire during spherical indentation. (a, b) Yield point. (c, d) Maximum indentation depth. X = [111]; Y = $[11\bar{2}]$; Z = $[\bar{1}10]$.

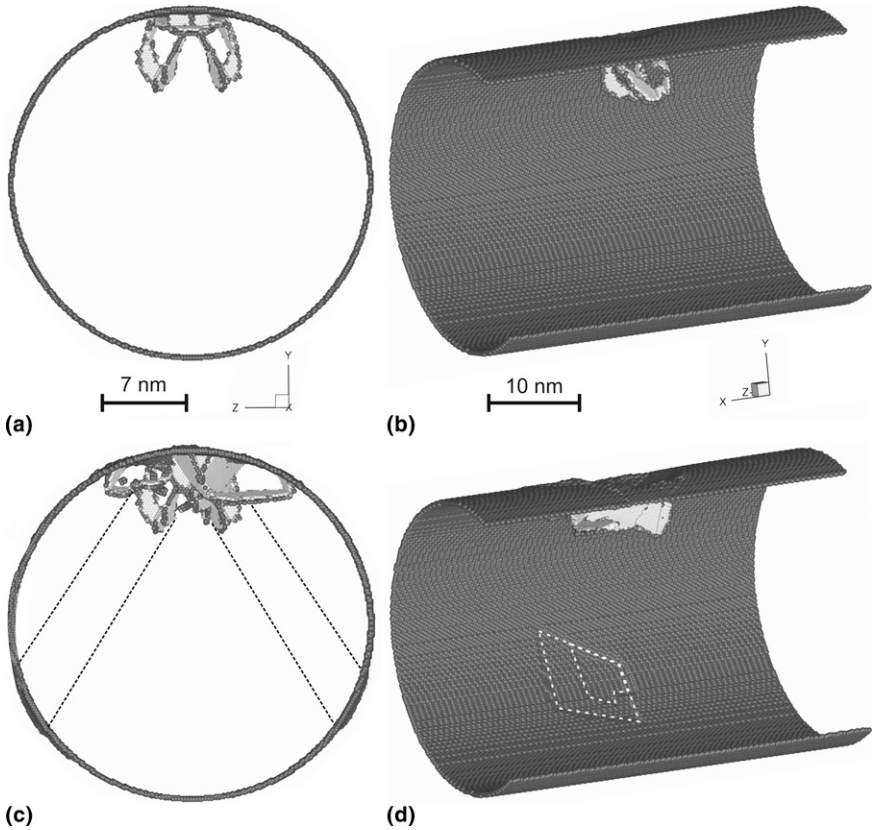

FIG. 6. Atomic-level representation of plastic deformation in a 30-nm-diameter Ni nanowire during spherical indentation. (a, b) Yield point. (c, d) Maximum indentation depth. Dashed lines represent the trajectory of prismatic dislocation loops escaping at free surfaces. X = [111]; Y = [11$\bar{2}$]; Z = [$\bar{1}$10].

TABLE II. Number of dislocations nucleated and absorbed by free surfaces for each nanowire.

Diameter (nm)	Half-dislocation loops nucleated	Half-dislocation loops absorbed by free surface	Four-sided prismatic loops formed	Four-sided prismatic loops absorbed by free surface
12	11	6	0	0
30	10	1	3	3

absorbs half-dislocation loops, whereas, in the 30-nm nanowire, the absorbed dislocations are primarily prismatic loops. In addition, Fig. 7(b) reveals that the newly nucleated dislocations are rapidly absorbed by the surface in the 12-nm nanowire before being able to form an entire prism. As illustrated in Fig. 7(c), this effect can be understood by the fact that the minimum distance needed to form full prismatic loops in the large nanowire ($\sim$10.3 nm) is almost identical to the size of the small nanowire.

IV. DISCUSSION

Recent studies in the literature[14,20,35,36] have shown that the size dependence on the Young's modulus of nanowires is related to surface stress effects, which cause the surface to become either softer or stiffer than the core of the nanowire. However, Liang et al.,[35] who have studied the influence of sample size on the Young's modulus of Cu nanowires, have found that size effects on elasticity are less significant for nanowires oriented along the [111] direction than other crystallographic directions. This effect results from the fact that the atom interactions on the (1-1 0) surface are inherently suppressed, which makes the surface elasticity effects more negligible for [111] metal nanowires.[35] Similarly, in the present study, the effect of sample size on the Young's modulus of [111]-oriented Ni nanowires during indentation was found to be negligible, which is in good agreement with Liang et al.'s study obtained under uniaxial deformation. As a result, the variations in slope observed along the $P - \delta$ nanoindentation curves in the elastic regime for nanowires (Fig. 2) mainly stem from the dependence of the slope on the nanowire radius. Such dependence was accurately predicted using Eq. (3) from the Hertz theory with a Young's modulus of 291 $\pm$ 7.5 GPa. In the elastic regime, the evolution of the contact pressures during indentation, as shown in Fig. 3, were similar between thin films and nanowires regardless of the sample size.

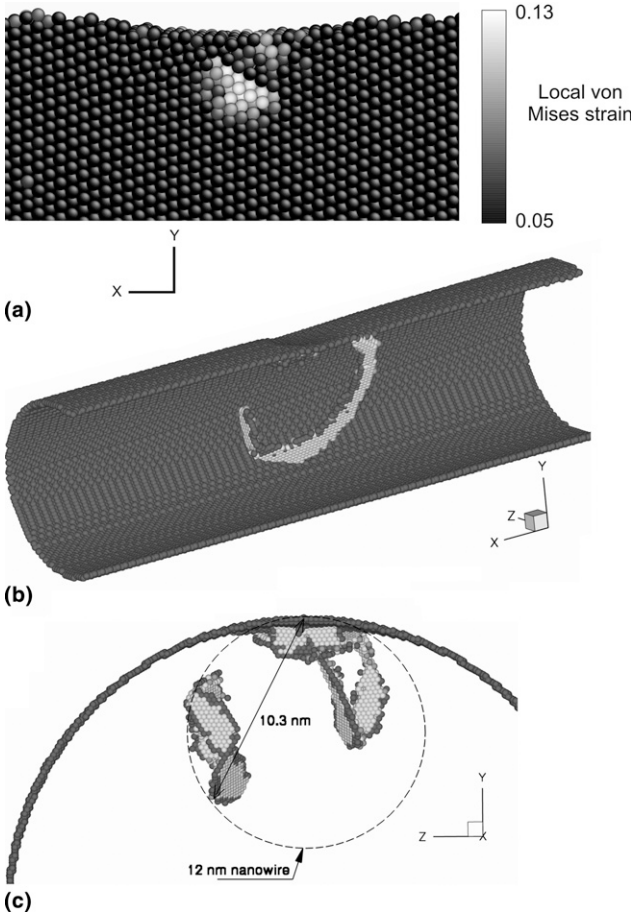

FIG. 7. Yielding and post-yielding deformation mechanisms in Ni nanowires. (a) Local von Mises strain at the yield point indicating homogeneous dislocation nucleation in the 12-nm nanowire. (b) Instantaneous absorption of the first half-dislocation loop in the 12-nm nanowire. (c) Creation and propagation of the first four-sided prismatic loop in the 30-nm nanowire, in comparison with the size of the 12-nm nanowire (dashed line).

Another essential result of our simulations is that no significant change in contact pressure is observed at the yield point during indentation in all thin films and nanowires investigated ($p_m = 30.6 \pm 1.5$ GPa). This observation seems to be in line with the atomistic results of Nair et al.,[37] who have also predicted that the contact pressure necessary to emit the first dislocation during spherical indentation in [111]-oriented Ni films does not significantly vary with the film thickness. Therefore, our simulations confirm that the same yield criterion operates during spherical indentation of thin films and nanowires with the presence of free boundaries. This result is also supported by the atomic-level analysis of deformation mechanisms at yield point, which shows the same mechanism of dislocation nucleation characterized by the emission of {111}<110> half-dislocation loops under the indenter; for example, see Figs. 4(c) and 6(a). Figure 7(a), which represents the local von Mises strain under the indenter in the 12-nm-diameter nanowire just before the yield point, reveals that the dislocation mechanism is homogeneous via the nucleation of a dislocation inside the sample. The same mechanism was observed in the other simulations regardless of the sample size. This result, coupled with the observation that the same number of dislocations was nucleated in nanowires of different size (see Table II), further suggests that the process of dislocation nucleation is not significantly affected by the free boundaries in the nanowires.

A key result of our simulations appears in the post-yielding regime, where the behavior of the 12-nm nanowire is markedly different from that of the 30-nm nanowire, as shown in Fig. 3(b) for a penetration depth larger than 0.8 nm. The hardness of the nanowires is found to decrease as the sample diameter decreases, which leads to an important softening effect for the smaller nanowire. In contrast, no significant size effect on the hardness has been found in thin films with a thickness of either 12 or 30 nm. In addition, the number of prismatic loops blocked by the fixed boundary shows no effects on the intrinsic hardness of thin films as represented in Fig. 3(a).

A review of the nanoindentation literature on nanowires[14–22] does not allow us to directly compare the present results with any experimental trend because the type and size of nanowires tested experimentally are different. However, it is worth mentioning that strong softening effects from free edges have also been observed in the indentation of patterned lines in single-crystal Al and polycrystalline Cu.[39–42] These experimental studies have shown a significant increase of indentation compliance and plastic deformation in metal lines because the line width was decreased in the micrometer range, which is somewhat similar to our observation of size dependence in Ni nanowires during spherical indentation. In particular, Choi and Suresh[42] found no length-scale effect on the elastic indentation response of single-crystal Al lines on Si substrates prior to the first plastic event; however, narrower lines showed increased plastic deformation after yielding. To rationalize the effect of line width, these authors proposed a model based on the extension of equilibrium dislocation position and the distance over which the dislocations approach the free surface of the side walls of the lines.

A similar mechanistic reasoning may be used here on nanowires, because the complex interaction between lattice dislocations escaping the crystal and free boundaries seems to be a predominant factor in the size dependence of the hardness of Ni nanowires, as opposed to the process of dislocation nucleation itself [Fig. 3(b)]. A caveat with this analysis is that the size variation in our nanowire models is several orders of magnitude less than that in Choi and Suresh's samples with micrometer metal lines. However, our simulations point to two fundamental changes in post-yielding

mechanisms as the size of the nanowire decreases. First, the small size of the 12-nm nanowire limits the extension of half-dislocation loops after nucleation and prevents their transformation into full prismatic loops, as shown in Figs. 7(b) and 7(c). As a result, it can be observed in Fig. 3(b) that the rate at which those dislocations are absorbed by the free surface is more significant in the small nanowire. Second, the absorption effect is only found to be relevant when several dislocations glide on the same slip system and exit at the same location on the surface of the nanowire. It is important to note that this mechanism also applies to the 30-nm nanowire, which was found to exhibit the same hardness than thin films (~21 GPa) regardless of the number of prismatic loops nucleated beneath the indenter, until two of these loops could escape the crystal at the same surface location [Fig. 6(d)]. However, it is clearly evident that the height of the surface steps, which is determined by the number of dislocations exiting the crystal at a same absorption site, is different between the two nanowires, as shown in Figs. 5(c) and 6(c). It is worth mentioning here that past atomistic simulations have predicted that a ½[110] step on the surface of a [111]-oriented single-crystal nanowire could lower its tensile yield stress by up to 38%.[43] This result may support the idea that the formation of surface steps upon dislocation absorption by the free surface is a controlling factor in the plasticity of nanowires. Therefore, it may be helpful to conduct further analysis of surface stresses in the vicinity of absorption sites and surface steps to gain more quantitative insight into the size dependence of crystal plasticity in metal nanowires during indentation.

V. CONCLUSIONS

Molecular dynamics simulations of spherical indentation on nanowires and thin films have been performed to characterize the influences of sample size and free-surface boundaries on the elastic properties and nanoindentation hardness of single-crystal Ni. In this study, particular focus was placed on [111]-oriented, dislocation-free Ni nanowires with a diameter of 12 and 30 nm. The main conclusions of this investigation can be summarized as follows:

(1) The nanoindentation response for both thin films and nanowires in the elastic regime was found to obey a Hertzian behavior. The mean value of Young's modulus for all samples was found equal to 291 ± 7.5 GPa, which showed that the sample size had no noticeable effect on the elastic properties of the nanowires during indentation.

(2) No significant change in mean contact pressure and underlying deformation mechanisms at yield point was observed between the samples. The mean contact pressure at the limit of elasticity was found equal to 30.6 ± 1.5 GPa. The simulations tend to confirm that the same yield criterion operates during spherical indentation of thin films and nanowires. The onset of plasticity was characterized by the same pattern of deformation at atomic level, which corresponded to the homogeneous nucleation of {111}<110> dislocation loops from the sample, regardless of the sample size.

(3) In the plastic regime, the hardness of Ni nanowires was found to be size dependent, such that the nanowire became softer as the wire diameter decreased. In contrast, no significant size effect of hardness was revealed in thin films as a function of the film thickness. The hardness of the films was on the order of 21 GPa for penetration depths larger than 0.8 nm. The processes of dislocation absorption by free-surface boundaries were shown to play a predominant role in the size effects of hardness in single-crystal Ni nanowires. The significance of softening effects in nanowires appeared to be correlated with the number of prismatic loops and {111} dislocation loops that escaped the crystal on identical slip systems.

The atomistic simulations presented here allow us to conclude that size effects on the mechanical properties of sub-100 nm metal nanowires may be studied experimentally using sharp indentation probes, such as depth-sensing nanoindentation[18] or atomic force microscopy-based indentation.[44]

ACKNOWLEDGMENTS

Support from the National Science Foundation (NSF) CAREER program (Grant No. DMR-0747658) and the computational resources provided by the Vermont Advanced Computing Center, which is supported by NASA (Grant No. NNX 06AC88G), are gratefully acknowledged. The simulations presented in this work were performed using LAMMPS molecular simulator.[45]

REFERENCES

1. M. Tian, J. Wang, J. Kurtz, T.E. Mallouk, and M.H.W. Chan: Electrochemical growth of single-crystal metal nanowires via a two-dimensional nucleation and growth mechanism. *Nano Lett.* **3,** 919 (2003).
2. J.J. Mock, S.J. Oldenburg, D.R. Smith, D.A. Schultz, and S. Schultz: Composite plasmon resonant nanowires. *Nano Lett.* **2,** 465 (2002).
3. A. Husain, J. Hone, H.W.Ch. Postma, X.M.H. Huang, T. Drake, M. Barbic, A. Scherer, and M.L. Roukes: Nanowire-based very-high-frequency electromechanical resonator. *Appl. Phys. Lett.* **83,** 1240 (2003).
4. L.A. Bauer, N.S. Birenbaum, and G.J. Meyer: Biological applications of high aspect ratio nanoparticles. *J. Mater. Chem.* **14,** 517 (2004).
5. C.J. Barrelet, A.B. Greytak, and C.M. Lieber: Nanowire photonic circuit elements. *Nano Lett.* **4,** 1981 (2004).

6. M.D. Uchic, D.M. Dimiduk, J.N. Florando, and W.D. Nix: Sample dimensions influence strength and crystal plasticity. *Science* **305,** 986 (2004).
7. J. Greer, W.C. Oliver, and W.D. Nix: Size dependence of mechanical properties of gold at the micron scale in the absence of strain gradients. *Acta Mater*. **53,** 1821 (2005).
8. B. Wu, A. Heidelberg, and J.J. Boland: Mechanical properties of ultrahigh-strength gold nanowires. *Nat. Mater*. **4,** 525 (2005).
9. D.M. Dimiduk, M.D. Uchic, and T.A. Parthasarathy: Size-affected single-slip behavior of pure nickel microcrystals. *Acta Mater*. **53,** 4065 (2005).
10. J.R. Greer and W.D. Nix: Nanoscale gold pillars strengthened through dislocation starvation. *Phys. Rev. B: Condens. Matter* **73,** 245410 (2006).
11. C.A. Volkert and E.T. Lilleodden: Size effects in the deformation of sub-micron Au columns. *Philos. Mag*. **86,** 5567 (2006).
12. H. Tang, K.W. Schwarz, and H.D. Espinosa: Dislocation escape-related size effects in single-crystal micropillars under uniaxial compression. *Acta Mater*. **55,** 1607 (2007).
13. Z.W. Shan, R.K. Mishra, S.A. Syed Asif, O.L. Warren, and A.M. Minor: Mechanical annealing and source-limited deformation in submicrometre-diameter Ni crystals. *Nat. Mater*. **7,** 115 (2008).
14. G. Stan, C.V. Ciobanu, P.M. Parthangal, and R.F. Cook: Diameter-dependent radial and tangential elastic moduli of ZnO nanowires. *Nano Lett*. **7,** 3691 (2007).
15. M. Lucas, A.M. Leach, M.T. McDowell, S.E. Hunyadi, K. Gall, C.J. Murphy, and E. Riedo: Plastic deformation of pentagonal silver nanowires: Comparison between AFM nanoindentation and atomistic simulations. *Phys. Rev. B: Condens. Matter* **77,** 245420 (2008).
16. D. Lee, M. Zhao, X. Wei, X. Chen, S.C. Jun, J. Hone, E.G. Herbert, W.C. Oliver, and J.W. Kysar: Observation of plastic deformation in freestanding single crystal Au nanowires. *Appl. Phys. Lett*. **89,** 111916 (2006).
17. X. Li, H. Gao, C.J. Murphy, and K.K. Caswell: Nanoindentation of silver nanowires. *Nano Lett*. **3,** 1495 (2003).
18. G. Feng, W.D. Nix, Y. Yoon, and C.J. Lee: A study of the mechanical properties of nanowires using nanoindentation. *J. Appl. Phys*. **99,** 074304 (2006).
19. X. Tao and X. Li: Catalyst-free synthesis, structural, and mechanical characterization of twinned $Mg_2B_2O_5$ nanowires. *Nano Lett*. **8,** 505 (2008).
20. H. Zhang, J. Tang, L. Zhang, B. An, and L.C. Qin: Atomic force microscopy measurement of the Young's modulus and hardness of single LaB_6 nanowires. *Appl. Phys. Lett*. **92,** 173121 (2008).
21. S. Bansal, E. Toimil-Molares, A. Saxena, and R.R. Tummala: Nanoindentation of single crystal and polycrystalline copper nanowires. *Elec. Comp. Tech. Conf*. **1,** 71 (2005).
22. T.H. Fang and W.J. Chang: Nanolithography and nanoindentation of tantalum-oxide nanowires and nanodots using scanning-probe microscopy. *Physica B (Amsterdam)* **352,** 190 (2004).
23. E. Rabkin and D.J. Srolovitz: Onset of plasticity in gold nanopillar compression. *Nano Lett*. **7,** 101 (2007).
24. E. Rabkin, H-S. Nam, and D.J. Srolovitz: Atomistic simulation of the deformation of gold nanopillars. *Acta Mater*. **55,** 2085 (2007).
25. K.A. Afanasyev and F. Sansoz: Strengthening in gold nanopillars with nanoscale twins. *Nano Lett*. **7,** 2056 (2007).
26. T. Zhu, J. Li, A. Samanta, A. Leach, and K. Gall: Temperature and strain-rate dependence of surface dislocation nucleation. *Phys. Rev. Lett*. **100,** 025502 (2008).
27. A. Cao and E. Ma: Sample shape and temperature strongly influence the yield strength of metallic nanopillars. *Acta Mater*. **56,** 4816 (2008).
28. Y. Mishin, D. Farkas, M.J. Mehl, and D.A. Papaconstantopoulos: Interatomic potentials for monoatomic metals from experimental data and ab initio calculations. *Phys. Rev. B: Condens. Matter* **59,** 3393 (1999).
29. E.T. Lilleodden, J.A. Zimmerman, S.M. Foiles, and W.D. Nix: Atomistic simulations of elastic deformation and dislocation nucleation during nanoindentation. *J. Mech. Phys. Solids* **51,** 901 (2003).
30. D. Feichtinger, P.M. Derlet, and H. Van Swygenhoven: Atomistic simulations of spherical indentations in nanocrystalline gold. *Phys. Rev. B: Condens. Matter* **67,** 024113 (2003).
31. G.J. Ackland and A.P. Jones: Applications of local crystal structure measures in experiment and simulation. *Phys. Rev. B: Condens. Matter* **73,** 054104 (2006).
32. K.L. Johnson: *Contact Mechanics* (Cambridge University Press, Cambridge, UK, 1985).
33. M.A. Meyers and K.K. Chawla: *Mechanical Behavior of Materials* (Prentice Hall, Upper Saddle River, NJ, 1999).
34. J. Li: AtomEye: An efficient atomistic configuration viewer. *Modell. Simul. Mater. Sci. Eng*. **11,** 173 (2003).
35. H. Liang, M. Upmanyu, and H. Huang: Size-dependent elasticity of nanowires: Nonlinear effects. *Phys. Rev. B: Condens. Matter* **71,** 241403 (2005).
36. S. Cuenot, C. Frétigny, S. Demoustier-Champagne, and B. Nysten: Surface tension effect on the mechanical properties of nanomaterials measured by atomic force microscopy. *Phys. Rev. B: Condens. Matter* **69,** 165410 (2004).
37. A.K. Nair, E. Parker, P. Gaudreau, D. Farkas, and R.D. Kriz: Size effects in indentation response of thin films at the nanoscale: A molecular dynamics study. *Int. J. Plast*. **24,** 2016 (2008).
38. J. Li, K.J. Van Vliet, T. Zhu, S. Yip, and S. Suresh: Atomistic mechanisms governing elastic limit and incipient plasticity in crystals. *Nature* **418,** 307 (2002).
39. Y. Choi, K.J. Van Vliet, J. Li, and S. Suresh: Size effects on the onset of plastic deformation during nanoindentation of thin films and patterned lines. *J. Appl. Phys*. **94,** 6050 (2003).
40. Y.A.M. Soifer, A. Verdyan, M. Kazakevich, and E. Rabkin: Edge effect during nanoindentation of thin copper films. *Mater. Lett*. **59,** 1434 (2005).
41. A.M. Minor, J.W. Morris, Jr., and E.A. Stach: Quantitative in situ nanoindentation in an electron microscope. *Appl. Phys. Lett*. **79,** 1625 (2001).
42. Y. Choi and S. Suresh: Nanoindentation of patterned metal lines on a Si substrate. *Scr. Mater*. **48,** 249 (2003).
43. B. Hyde, H.D. Espinosa, and D. Farkas: An atomistic investigation of elastic and plastic properties of Au nanowires. *JOM* **57,** 62 (2005).
44. F. Bedoui, F. Sansoz, and N.S. Murthy: Incidence of nanoscale heterogeneity on the nanoindentation of a semicrystalline polymer: Experiments and modeling. *Acta Mater*. **56,** 2296 (2008).
45. S.J. Plimpton: Fast parallel algorithms for short-range molecular-dynamics. *J. Comput. Phys*. **117,** 1 (1995).